

Probing photocarrier dynamics of pressurized graphene using time-resolved terahertz spectroscopy

Yunfeng Wang(王云峰), Shujuan Xu(许淑娟), Jin Yang(杨金), and Fuhai Su(苏付海)
Citation: Chin. Phys. B, 2023, 32 (**6**): 067802. DOI: 10.1088/1674-1056/acc2b1
Journal homepage: http://cpb.iphy.ac.cn; http://iopscience.iop.org/cpb

What follows is a list of articles you may be interested in

Graphene metasurface-based switchable terahertz half-/quarter-wave plate with a broad bandwidth

Xiaoqing Luo(罗小青), Juan Luo(罗娟), Fangrong Hu(胡放荣), and Guangyuan Li(李光元)
Chin. Phys. B, 2023, 32 (**2**): 027801. DOI: 10.1088/1674-1056/ac80a8

Dynamically controlled asymmetric transmission of linearly polarized waves in VO_2-integrated Dirac semimetal metamaterials

Man Xu(许曼), Xiaona Yin(殷晓娜), Jingjing Huang(黄晶晶), Meng Liu(刘蒙), Huiyun Zhang(张会云), and Yuping Zhang(张玉萍)
Chin. Phys. B, 2022, 31 (**6**): 067802. DOI: 10.1088/1674-1056/ac4bd3

Optically tuned dielectric characteristics of $SrTiO_3$/Si thin film in the terahertz range

Bin Zou(邹斌), Qing-Qing Li(李晴晴), Yu-Ping Yang(杨玉平), and Hai-Zhong Guo(郭海中)
Chin. Phys. B, 2021, 30 (**10**): 107802. DOI: 10.1088/1674-1056/ac04a7

High performance terahertz anisotropic absorption in graphene-black phosphorus heterostructure

Jinming Liang(梁晋铭), Jiangtao Lei(雷江涛), Yun Wang(汪云), Yan Ding(丁燕), Yun Shen(沈云), Xiaohua Deng(邓晓华)
Chin. Phys. B, 2020, 29 (**8**): 087805. DOI: 10.1088/1674-1056/ab9cbf

Temperature dependent terahertz giant anisotropy and cycloidal spin wave modes in $BiFeO_3$ single crystal

Fan Liu(刘凡), Zuanming Jin(金钻明), Xiumei Liu(刘秀梅), Yuqing Fang(方雨青), Jiajia Guo(国家嘉), Yan Peng(彭滟), Zhenxiang Cheng(程振祥), Guohong Ma(马国宏), Yiming Zhu(朱亦鸣)
Chin. Phys. B, 2020, 29 (**7**): 077804. DOI: 10.1088/1674-1056/ab8dae

---

Probing photocarrier dynamics of pressurized graphene using time-resolved terahertz spectroscopy

Yunfeng Wang(王云峰)[1,2], Shujuan Xu(许淑娟)[1], Jin Yang(杨金)[1], and Fuhai Su(苏付海)[1,†]

[1] *Key Laboratory of Materials Physics, Institute of Solid State Physics, HFIPS, Chinese Academy of Sciences, Hefei* 230031, *China*
[2] *University of Science and Technology of China (USTC), Hefei* 230026, *China*

(Received 28 January 2023; revised manuscript received 25 February 2023; accepted manuscript online 9 March 2023)

Graphene hosts intriguing photocarrier dynamics such as negative transient terahertz (THz) photoconductivity, high electron temperature, benefiting from the unique linear Dirac dispersion. In this work, the pressure effects of photocarrier dynamics of graphene have been investigated using *in situ* time-resolved THz spectroscopy in combination with diamond anvil cell exceeding 9 GPa. We find that the negative THz conductivity maintains in our studied pressure range both for monolayer and bilayer graphene. In particular, the amplitude of THz photoconductivity in monolayer graphene manifests an extraordinary dropping with pressure, compared with that from the counterparts such as bulk silicon and bilayer graphene. Concomitantly, the time constant is reduced with increasing pressure, highlighting the pressure-induced hot carrier cooling. The pressure dependence of photocarrier dynamics in monolayer graphene is likely related with the enhancement of the interfacial coupling between diamond surface and sample, allowing for the activity of new electron–phonon scattering. Our work is expected to provide an impetus for the studies of high-pressure THz spectroscopy of two-dimensional materials.

Keywords: terahertz, photocarrier dynamics, graphene, high pressure

PACS: 78.20.–e, 78.47.J–, 68.65.Pq, 07.35.+k **DOI:** 10.1088/1674-1056/acc2b1

1. Introduction

Ultrafast photoexcitaion in material enables an establishment of a transient hot carrier system, that is, the nonequibrium electronic subsystem featuring the quasi-Fermi–Dirac distribution (QFD) with electron temperature (T_e) higher than that of lattice subsystem (T_l), which is followed by the kinetics processes of energy exchange between phonon and electron.[1–5] The knowledge and understandings of hot carrier dynamics are crucial for the applications of devices involving the photovoltaic effect, light emission, photothermoelectric effect and others.[6,7] For example, if hot carriers can be harnessed before the energy is lost, it is expected to break the Shockley–Queisser limitation and facilitate the energy conversion in photovoltaic devices.[8,9] Graphene is found to be a prototypical Dirac semimetal that hosting hot carrier dynamics. Benefiting from the unique linear dispersion relationship, vanishing density of state (DOS) near Dirac point, small Fermi surface, and low electron heat capacity, the photoinjected carriers in graphene are prone to occupy the high-energy side in k space via the electron–electron scattering within a few tens femtoseconds.[10–15] Due to the electronic redistribution featuring with the high-energy tail far larger than the energy of excitation photon, the hot-carrier temperature approaching a few thousands Kelvins can be achieved in subpicosecond time scale under moderate photoexcitation level.[16] In particular, the hot-carrier dynamics are essential for the ultrafast photophysics in graphene including the energy transfer,[17–20] high-harmonic wave generation,[21,22] terahertz (THz) transport, and photothermoelectric effect. At ambient condition, the different methods such as transient absorption, time-resolved THz spectroscopy (TRTS), time- and angle-resolved photoemission spectroscopy (tr-ARPES), *etc.*[23–25] have been demonstrated to be powerful to decipher the photocarrier dynamics in graphene. Among them, TRTS serves as an ideal non-contact technique providing the information of photoconductivities both in frequency and time domain, which simultaneously reflects the intraband transport and interband recombination dynamics of photocarriers with a subpicosecond temporal resolution.[26–28] In graphene, TRTS have been utilized to unveil a mount of interesting phenomena related to the hot carrier dynamics such as the negative THz photoconductivity, the multiplication hot-carrier generation, ultrafast plasmon thermalization.[29–32]

Diamond anvil cell (DAC) is able to produce the hydrostatic pressure, and serves as a clean knob to continuously tune the interatomic interactions, leading to the modifications of the electronic and lattice structure in materials.[33] In recent years, a few pioneering works have been devoted to address the pressure effect on the physical properties of graphene.[34] Pressure may provide a unique route to convert the multilayer graphene to the diamond-like structures.[35,36] Ke *et al.* observed a semimetal-to-semiconductor transition in Bernal-stacked trilayer graphene above 30 GPa, and achieved the maximum intrinsic bandgap of 2.5 ± 0.3 eV through the pressure tuning.[37] Tao *et al.* studied the pressure dependence of Raman modes of bilayer graphene up to 50 GPa, and identi-

†Corresponding author. E-mail: fhsu@issp.ac.cn

© 2023 Chinese Physical Society and IOP Publishing Ltd

fied a transition from sp^2 to metastable sp^3 bonding at high pressure when the water was taken as the pressure transmission medium (PTM).[38] On the other hand, regulating the hot-carrier dynamics has fundamental significance for the development of photoelectric and electric devices such as the terahertz (THz) emitter, lightharvesting, high-frequency electronics. Pressure tuning on ultrafast dynamics including the Auger recombination,[39] thermal transport,[40] and hot carrier cooling[41,42] have been reported. For instance, basing on the femtosecond pump–probe optical spectroscopy, it was found that the external hydrostatic pressure could effectively reduce the cooling time of hot carrier in bilayer graphene by enhancing the interlayer coupling and providing a new energy dissipation channel stemming from interlayer phonon modes.[41] In addition, the direct accesses into the photocarrier dynamics in THz frequency under pressure have been demonstrated using the TRTS in combination with DAC in recent years.[43] However, the THz photophysics under pressure in two-dimensional (2D) material with atomic thickness have not been addressed so far. In this work, we take the graphene as the testbed, and perform the TRTS under pressure above 9 GPa. We reveal that the THz transmission and photo-induced THz conductivity remain nearly constant and negative in our studied pressure range, respectively, while the amplitude and relaxation time constants for THz photoconductivity from monolayer graphene are reduced with pressure. Our work shows the feasibility probing the photocarrier dynamics under pressure for ultrathin 2D material using TRTS, which is expected to facilitate the developments of the high-pressure THz spectroscopy.

2. Experiments

DAC (Fig. 1(a)) with a culet size of 1000 μm was used to exert the external hydrostatic pressure. The aperture of the drilled stainless steel gasket was about 400 μm in diameter. The methods for sample fabrication and loading are similar as in reference were applied.[41] In briefly, the monolayer and bilayer graphene films on CuNi alloy substrate were fabricated using chemical vapor deposition (CVD) method. The polymethyl methacrylate (PMMA) assisted method was employed to transfer the graphene films onto the diamond of DAC. For the measurement of bulk silicon, a piece of undoped silicon single crystal wafer was polished into a thin-platelet sample with a size around 200 μm × 200 μm and thickness of about 10 μm before being loaded in the DAC. Silicon oil was utilized as PTM and the value of pressure was gauged by means of the photoluminescence of ruby balls.

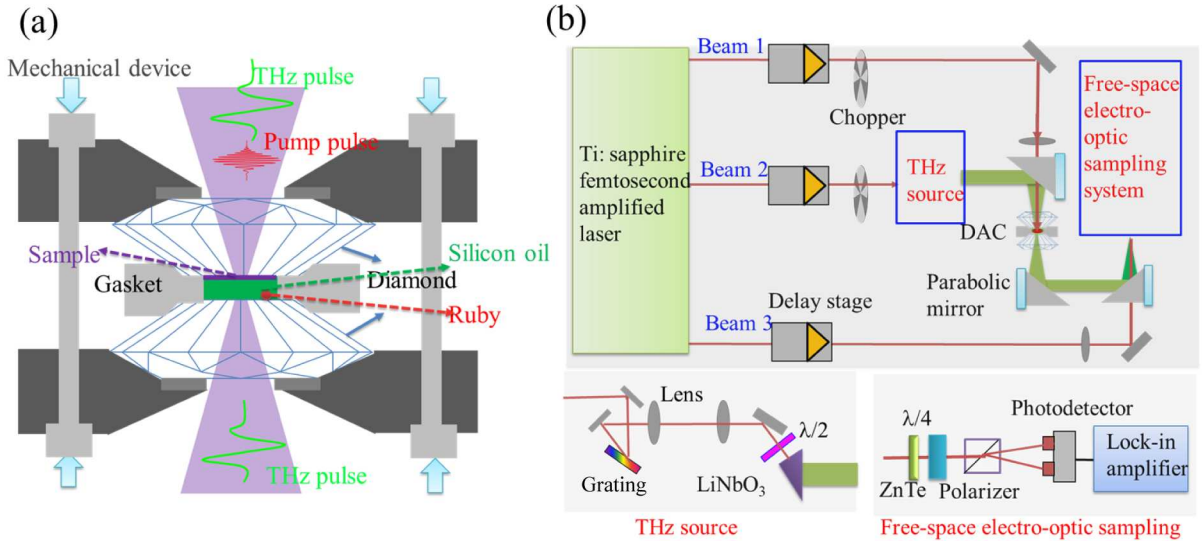


Fig. 1. (a) Schematic diagram of DAC apparatus for *in-situ* TRTS. (b) Optical layout of the TRTS setup.

The experimental scheme for TRTS measurement was plotted in Fig. 1(b). An amplified Ti:sapphire laser (Coherent Legend) was used as the source, which deliver the femtosecond pulses with average power of 4.0 W, duration of 45 fs, central wavelength of 800 nm, repetition of 1 kHz. The laser beam was divided into three portions for the generation and sampling of THz pulses, as well as for the photoexcitation of the sample in DAC, respectively. THz pulses with the average power of 300 mW were generated from an $LiNbO_3$ prism using tilted-pulse front technique;[44,45] the laser beam with power of 2 W was dispersed by a grating with the groove density of 1800 gr/mm, and then was imaged onto the $LiNbO_3$ crystal through a 4f lens assembly. The THz beam was focused onto the sample in DAC via the off-axis parabolic mirrors assembly. The THz signal passing through the sample was collected by the ZnTe detection crystal with 1-mm thickness, by which the THz waveform was gated using the free-space electro-optic sampling technique. For the photoexciation, the DAC chamber with sample was globally illuminated by the pump beam with the wavelength of 800 nm. In the measure-

ment, the lock-in amplifiers were applied to record the voltage signal from the balanced photodetector. The optical chopper was placed in either the THz beam path for the sampling of the THz waveform or the optical pump path in order to detect the photoinduced transmission change. The laser pulses were synchronized in time by the motorized stages with retroreflector mirrors. The time evolution of differential THz transmission was measured by varying the time delay between the pump pulse and THz pulse, while keeping the delay of optical gating pulse with respect to the THz pulse fixed. All the TRTS experiments were performed at room temperature. The applied pump fluences incident on the DAC were kept below 50 μJ/cm^2 to avoid the multiphoton absorption from diamonds. We also examined the differential THz transmission with photoexcitation for the DAC only with PTM under high pressure. No any photoinduced modulation of THz transmission signal could be observed.

3. Results and discussion

In Fig. 2(a), we show the THz waveform passing through monolayer graphene in DAC without photoexcitation at different pressure. The corresponding spectrum extracted through fast Fourier transform (FFT) at each pressure is plotted in Fig. 2(b). It should be mentioned that the THz-electric-field induced nonlinear absorption in graphene should be negligible because about 80% of THz energies are blocked by the DAC apparatus. As can be seen, the THz transmission does not exhibit significant changes both in time and frequency domain with pressure. Since no recognizable shrink or expansion occurs to the clear aperture of the DAC in the studied pressure range, it indicates the pressure dependence of the THz transmission reflect the intrinsic properties of graphene. Such pressure independence of THz transmission signifies that the highly stability of electronic and lattice structure for graphene at the pressure below 10 GPa, which is consistent with previous results obtained using the experimental methods such as Raman spectroscopy and electric transport.[37]

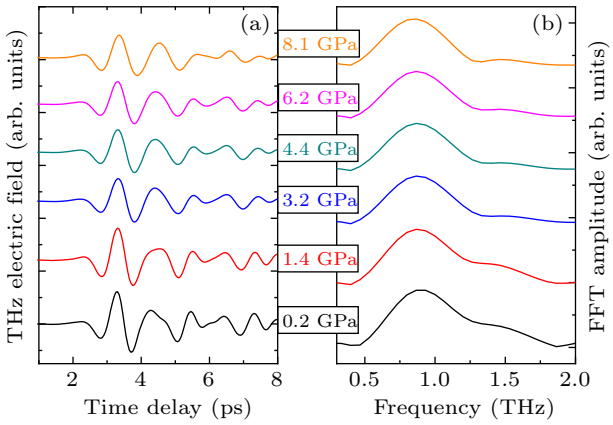


Fig. 2. (a) Transmitted THz waveform through monolayer graphene in DAC at different pressures, (b) corresponding FFT spectrum for each pressure.

TRTS allow us to directly track the time evolution of the photo-induced modulation in the THz transmission, that is, $\Delta T(t_p) = T(t_p) - T_0(t_p)$, by varying the time delay (t_p) between THz and pump pulses. Here the T and T_0 denotes the THz peak transmission with and without photoexcitation, respectively. In Fig. 3, we presents the differential THz transmission (DTT), $-\Delta T/T_0$, as the function of time delay (t_p) at different pressures. In our study, the sample system can be considered as the graphene film on the diamond substrate. In this case, the DTT is proportional with the photo-induced variety of the real part of sheet conductivity ($\mathrm{Re}\,\Delta\sigma$), *i.e.*,

$$-\frac{\Delta T}{T_0}(t_p) = \frac{\mathrm{Re}\,\Delta\sigma(t_p)\,Z_0}{1+n_s}.$$

Here n_s and Z_0 represent the THz refractive index of diamond and the impedance of the free space, respectively. At ambient condition, the photoexcitation is able to induce the negative (positive) THz photoconductivity due to the intraband carrier heating (interband electron–hole injection), depending on the Fermi level (or doping level) of graphene. To determine the sign of the DTT, we measured TRTS for undoped bulk silicon under pressure by keeping the parameters of lock-in amplifier unchanged. Because silicon maintains semiconductor phase below 10 GPa, the photoexcitation using 800-nm photons tend to generate the electron–hole pairs and increase the THz conductivity, leading to the positive photoconductivity (negative DTT). As shown in Fig. 3(a), the sign of DTT of silicon is opposite with that of graphene under pressure. This substantiates that the THz photoconductivity of graphene holds negative in our studied pressure range. The main feature revealed in Fig. 2 is that the amplitude of DTT is pronouncedly reduced with elevating pressure, *e.g.*, the peak magnitude of DTT is declined by a factor of three at the pressure of 3.2 GPa compared with that obtained at low pressure (0.2 GPa). Indeed, the attenuation magnitude of DTT signal with pressure even approaches that in bulk silicon as exemplified by Fig. 3(a). Since the THz transmission without photoexcitation almost keep constant under pressure as discussed above, such reduction of the DTT amplitude is nontrivial in view of the atomic layer thickness of graphene. Although the amplitude does not manifest obvious change in the pressure range between 3.2 GPa and 6.2 GPa, the DTT signal totally disappears as the pressure is above 8 GPa. Different mechanisms for the negative THz photoconductivity (positive DTT) of graphene have been proposed. For instance, the earlier works suggested that the photoinduced population inversion near the Dirac point, in concomitant with the stimulated THz emission contributed to the reduction of THz photoconductivity.[46] Tielrooij *et al.* evidenced that the generation of the secondary hot carrier could play key role for the negative THz photoconductivity. Furthermore, the correlations between THz pho-

toconductivity and Fermi energy or doping level were thoroughly interrogated, which unveiled the microscopic pictures underlying the negative THz photoconductivity, including the enhancement of carrier–carrier scattering due to the high electron temperature, the increase in carrier–impurity scattering stemming from the reduction of long-range Coulomb screening. In addition, the carrier temperature dependence of optical phonon scattering was also proposed to be possible reason for negative THz photoconductivity.[47] Overall, the origins of the negative THz photoconductivity have close correspondences with the hot carrier. The high-energy carrier redistribution upon photoexcitation allows for the activities of multiple cooling channels involving the carrier–carrier scattering, carrier-optical phonon scattering, carrier–impurity scattering, as well as the electron temperature regulation on these scattering processes. To understand the pressure effect of the DTT transient, we first take into account the change of optical absorption coefficient with pressure. Indeed, the electronic structure of graphene is demonstrated be very stable at low pressure range.[41] Thereby, the pressure dependence of optical absorption has negligible impaction on the THz photoconduction in our studied pressure region. Second, we need to consider the pressure effect of Fermi level. As indicated in previous reports, the reduction of Fermi level can help to decrease the weight of negative THz photoconductivity. If the drop of DTT amplitude with pressure is a consequence of the shift of Fermi level, it is expected that the switching from negative to positive in the sign of DTT takes place above 8.2 GPa. However, we do not observe the emergence of positive DTT signal even at higher pressure. As a result, the factor related with Fermi level should be excluded. In addition, it was found that the pressure-induced augmentation of defect concentration contributed to the reduction of THz photoconduction in semiconductor such as bulk GaAs.[48] Such defect state evolution with pressure should also occur to bulk silicon as revealed in Fig. 3(a), where both DTT amplitude and photocarrier relaxation time is obviously reduced with increasing pressure. Nevertheless, the pressure effect of defect state in the photocarrier dynamics of graphene has proved to be insignificant.[41] Especially, the decay process of DTT transient does not continue to shorten above 4 GPa as shown in Fig. 5(a), which will be discussed later. This pressure behavior of photocarrier relaxation is contrast with that in bulk silicon. Therefore, the defect effect under pressure cannot explain the pressure dependence of photocarrier dynamics in monolayer graphene. Herein, we propose that the pressure behavior of DTT has close correspondence with the enhancement of coupling between graphene film and diamond surface. With increasing pressure, the effective contact between graphene and DAC surface become stronger. Although the new bonding or orbital hybridization between the carbon atoms from graphene and diamond should not be formed below 10 GPa, the interface van der Waals force may be boosted in such pressure range. Consequently, the phonon modes associating with the interface vibration likely become robust at high pressure, and act as a new channel for electron scattering. As for the photocarrier dynamics in graphene, most studies pointed out that that the electron–electron (e–e) and electron–phonon (e–ph) interactions dominated the formation of hot electron and the energy relaxation. Upon ultrafast photoexcitation, the electron–hole pairs are injected or excited immediately via interband or intraband transitions, which is followed by a rapid thermalization through e–e scattering and e–ph scattering in subpicosecond, creating the QFD with higher T_e than T_L. The activity of more phonon modes likely participate in the hot electron redistribution and subsequent cooling, and is able to decrease the initial electron temperature under pressure, reducing the amplitude of DTT.[49] Noteworthily, the amplitude of DTT exhibits weak pressure dependence between 3.2 GPa and 6.2 GPa. We suggest that this pressure dependence is due to the nonhomogeneous effect both in graphene sample and hydrostatic pressure. On one hand, there exists the nonhomogeneous bubbles and wrinkles in graphene. On the other hand, the pressure distribution is also not spatially uniform for large sized diamond culet. As consequently, the enforcement of interface coupling between graphene and diamond surface does not manifest monotonous increasing trend with pressure.

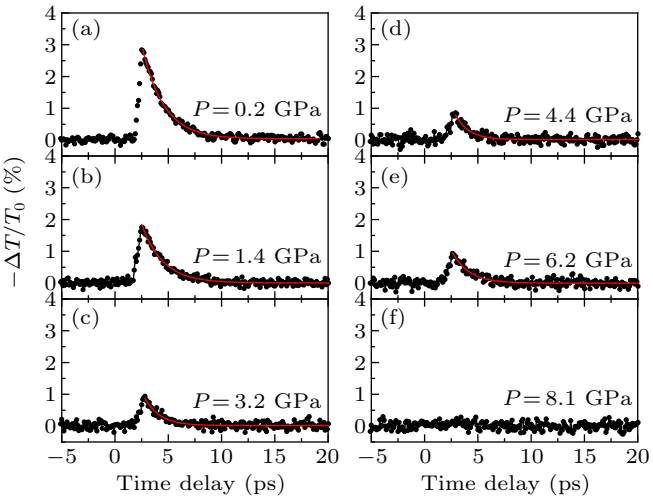


Fig. 3. The measured differential THz transmission (DTT) transients upon photoexcitation at different pressures for monolayer graphene.

To further examine the interfacial coupling effect, we measured the TRTS under pressure for double-layer graphene. In Fig. 2(b), we plotted the DTT transient at different pressure. In analogy with monolayer graphene, the sign of the DTT signal maintains positive in the studied pressure range, indicating the negative THz photoconductivity. Differently, the amplitude of DTT of bilayer graphene does not drop as rapidly as that in monolayer sample. In contrast with monolayer graphene, the peak of DTT still amounts to 0.2% at the

pressure of 9.8 GPa. Such relatively weak pressure dependence of DTT amplitude furthermore emphasize that the defect effect should not play important role for the photocarrier dynamics of pressurized graphene. Otherwise, the DTT amplitude should decline faster in bilayer graphene than that in monolayer graphene because the pressure-induced defect augmentation is expected to be more prominent while the layer number is increased. From the viewpoint of interfacial coupling effect, the increase in the thickness of graphene is favor of the relief of van der Waals interaction from diamond-sample interface. As a result, it is reasonable that the DTT amplitude of bilayer graphene is less sensitive to the external pressure compared with monolayer graphene. Therefore, our proposed interface coupling mechanism can provide a plausible interpretation for the pressure dependence of DTT amplitude in graphene.

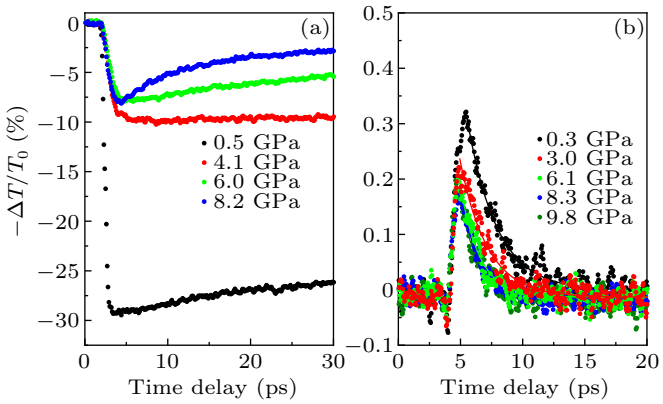


Fig. 4. The measured DTT transients upon photoexcitation at different pressures for (a) bulk silicon and (b) bilayer graphene at different pressures, respectively.

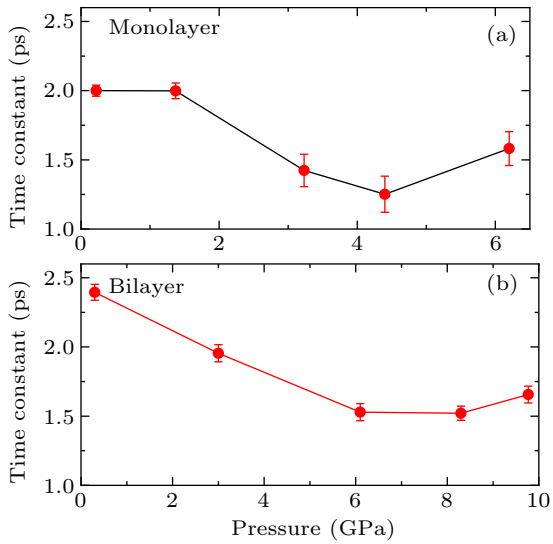


Fig. 5. The extracted time constant as a function of pressure for (a) monolayer graphene and (b) doube-layer graphene, respectively.

In the next, we proceed to analyze the pressure effects on the photocarrier relaxation in graphene, and interrogate if the interfacial coupling impacts the cooling process of hot carrier under pressure. In Figs. 5(a) and 5(b), we displayed the time constants *versus* pressure, which were extracted using the single-exponential function fittings for DTT curves of monolayer and bilayer graphene, respectively. For monolayer graphene, the time constant is initially reduced with increasing pressure, however, shows somewhat rising above 6 GPa. It implies that the cooling of photocarrier can be accelerated with the application of pressure. In general, the different phonon modes including the optical phonons, the acoustic phonons, as well as the disorder-assistant acoustic phonons (named as supercollision) are proposed to dominate the e–ph scattering and carrier cooling in graphene.[50–53] Especially, the high-frequency optical phonons participating in the carrier cooling can set a phonon bottleneck for the energy relaxation, *i.e.*, the optical phonon emission is less efficient as the energy of electron is lower than that of optical phonon. Thereby, the subsequent energy dissipation is dominated by the e–ph scatterings through low-frequency acoustic phonons, or supercollision.[54] Under ambient condition, the time scale for carrier cooling of graphene ranging from a few to a few hundred picoseconds, depending on the carrier density and temperature, have been reported.[55–57] Herein, we suggest that enhancement of graphene–diamond interfacial coupling under pressure allow for the activity of new phonon mode, provide a new channel for e–ph scattering. Such new scattering pathway may intermediate the e–ph interactions from the high-frequency optical phonon and low-frequency acoustic phonon, and then can suppress the hot phonon bottleneck to some extent, speeding up the carrier cooling. At higher pressure beyond 6 GPa, the phonon structure of monolayer graphene probably is changed and dominate the e–ph scattering again, *e.g.*, the frequency of optical phonon should be increased with pressure. The prolonging of relaxation dynamics above 6 GPa likely marks the robustness of the hot phonon bottleneck effect under pressure,[58] which need to be further investigated in future. As shown in Fig. 5(b), the carrier cooling process is also found to be shortened with elevating pressure in bilayer graphene. As discussed above, the effect of graphene–diamond interfacial coupling is relatively weak in comparison with monolayer graphene in DAC, which cannot account for the pressure dependence of time constant in bilayer graphene. Ni *et al.* found that the cooling time of hot carrier in bilayer graphene was pronouncedly decreased with increasing pressure, basing on the femtosecond near-infrared pump–probe spectroscopy. Furthermore, the interlayer phonon modes, *i.e.*, the shear and breathing vibrations, were evidenced to play vital roles for the hot carrier cooling at high pressure.[41] Our observed pressure behavior of photocarrier relaxation in bilayer graphene result is qualitatively consistent with this reported work although our current pressure range is low. The near-infrared pump–probe spectroscopy mainly track the time evolution of hot carrier distribution by probing the interband

transition. In contrast, the TRTS detects the photocarrier relaxation dynamics through monitoring the intrband transition benefiting from the small photon energy of THz pulse. Therefore, it is reasonable that the two methods have different sensitivities, and normally may give some discrepancies for the measured photocarrier dynamics.

4. Conclusion

In summary, we employed the TRTS in combination with DAC to investigate the photocarrier dynamics of graphene with the application of external hydrostatic pressure beyond 9 GPa. The photo-induced increase of THz transmission, signifying the negative THz conductivity, is found to maintain in the studied pressure range both for monolayer graphene and bilayer graphene. Interestingly, the amplitude of DTT from monolayer graphene shows extraordinary drop with pressure compared with that from counterparts such as bulk silicon and bilayer graphene. In addition, the relaxation time constant characterizing the hot carrier cooling manifests decreasing trend with pressure. We proposed that the enhancement of the interfacial interaction between diamond surface and graphene under pressure provides a new channel for e–ph scattering, which hinder the initial elevation of electron temperature and lead to the acceleration of cooling process of hot carrier in graphene. Our work establishes a benchmark for the understanding of ultrafast photophysics of graphene under pressure, and is expected to stimulate the studies of high-pressure THz spectroscopy of 2D materials.

Acknowledgments

Project supported by the National Natural Science Foundation of China (Grant Nos. 12174398, 12004387, 51727806, 51672279, 11874361, and 12204484), the Innovation Program of Chinese Academy of Sciences (Grant No. CXJJ-19-B08), the Youth Innovation Promotion Association of Chinese Academy of Sciences (Grant No. 2021446), the HFIPS Director's Fund of Chinese Academy of Sciences (Grant Nos. 2021YZGH03 and YZJJKX202202), and China Postdoctoral Science Foundation (Grant No. 2021M703255). We gratefully acknowledge professor Yanwu Zhu from USTC for his key supporting on the graphene samples preparation in this work.

References

[1] Gatamov R, Baydin A, Krzyzanowska H and Tolk N 2020 *Mater. Res. Express* **7** 095601
[2] George P A, Strait J, Dawlaty J, Shivaraman S, Chandrashekhar M, Rana F and Spencer M G 2008 *Nano Lett.* **8** 4248
[3] Sabbah A J and Riffe D M 2002 *Phys. Rev. B* **66** 165217
[4] Fann W S, Storz R, Tom H W K and Bokor J 1992 *Phys. Rev. B* **46** 13592
[5] Allen P B 1987 *Phys. Rev. Lett.* **59** 1460
[6] Gabor N M, Song J C W, Ma Q, Nair N L, Taychatanapat T, Watanabe K, Taniguchi T, Levitov L S and Jarillo-Herrero P 2011 *Science* **334** 648
[7] Tielrooij K J, Piatkowski L, Massicotte M, Woessner A, Ma Q, Lee Y, Myhro K S, Lau C N, Jarillo-Herrero P, van Hulst N F and Koppens F H L 2015 *Nat. Nanotechnol.* **10** 437
[8] Ross R T and Nozik A J 1982 *J. Appl. Phys.* **53** 3813
[9] Nelson C A, Monahan N R and Zhu X Y 2013 *Energy Environ. Sci.* **6** 3508
[10] Massicotte M, Soavi G, Principi A and Tielrooij K J 2021 *Nanoscale* **13** 8376
[11] Sun B Y, Zhou Y and Wu M W 2012 *Phys. Rev. B* **85** 125413
[12] Betz A C, Vialla F, Brunel D, Voisin C, Picher M, Cavanna A, Madouri A, Fève G, Berroir J M, Plaçais B and Pallecchi E 2012 *Phys. Rev. Lett.* **109** 056805
[13] Winnerl S, Orlita M, Plochocka P, Kossacki P, Potemski M, Winzer T, Malic E, Knorr A, Sprinkle M, Berger C, de Heer W A, Schneider H and Helm M 2011 *Phys. Rev. Lett.* **107** 237401
[14] Breusing M, Kuehn S, Winzer T, Malić E, Milde F, Severin N, Rabe J P, Ropers C, Knorr A and Elsaesser T 2011 *Phys. Rev. B* **83** 153410
[15] Butscher S, Milde F, Hirtschulz M, Malić E and Knorr A 2007 *Appl. Phys. Lett.* **91** 203103
[16] Pogna E A A, Jia X, Principi A, Block A, Banszerus L, Zhang J, Liu X, Sohier T, Forti S, Soundarapandian K, Terrés B, Mehew J D, Trovatello C, Coletti C, Koppens F H L, Bonn M, Wang H I, van Hulst N, Verstraete M J, Peng H, Liu Z, Stampfer C, Cerullo G and Tielrooij K J 2021 *ACS Nano* **15** 11285
[17] Fu S, du Fossé I, Jia X, Xu J, Yu X, Zhang H, Zheng W, Krasel S, Chen Z, Wang Z M, Tielrooij K J, Bonn M, Houtepen A J and Wang H I 2021 *Sci. Adv.* **7** eabd9061
[18] Zheng Q, Saidi W A, Xie Y, Lan Z, Prezhdo O V, Petek H and Zhao J 2017 *Nano Lett.* **17** 6435
[19] Virga A, Ferrante C, Batignani G, De Fazio D, Nunn A D G, Ferrari A C, Cerullo G and Scopigno T 2019 *Nat. Commun.* **10** 3658
[20] Lai J, Liu X, Ma J, Wang Q, Zhang K, Ren X, Liu Y, Gu Q, Zhuo X, Lu W, Wu Y, Li Y, Feng J, Zhou S, Chen J H and Sun D 2018 *Adv. Mater.* **30** 1707152
[21] Hafez H A, Kovalev S, Deinert J C, Mics Z, Green B, Awari N, Chen M, Germanskiy S, Lehnert U, Teichert J, Wang Z, Tielrooij K J, Liu Z, Chen Z, Narita A, Müllen K, Bonn M, Gensch M and Turchinovich D 2018 *Nature* **561** 507
[22] Baudisch M, Marini A, Cox J D, Zhu T, Silva F, Teichmann S, Massicotte M, Koppens F, Levitov L S, García de Abajo F J and Biegert J 2018 *Nat. Commun.* **9** 1018
[23] Huang L, Hartland G V, Chu L Q, Luxmi, Feenstra R M, Lian C, Tahy K and Xing H 2010 *Nano Lett.* **10** 1308
[24] Tielrooij K J, Song J C W, Jensen S A, Centeno A, Pesquera A, Zurutuza Elorza A, Bonn M, Levitov L S and Koppens F H L 2013 *Nat. Phys.* **9** 248
[25] Sun D, Divin C, Mihnev M, Winzer T, Malic E, Knorr A, Sipe J E, Berger C, de Heer W A, First P N and Norris T B 2012 *New J. Phys.* **14** 105012
[26] Li G, Amer N, Hafez H A, Huang S, Turchinovich D, Mochalin V N, Hegmann F A and Titova L V 2020 *Nano Lett.* **20** 636
[27] Titova L V, Cocker T L, Cooke D G, Wang X, Meldrum A and Hegmann F A 2011 *Phys. Rev. B* **83** 085403
[28] Beard M C, Turner G M and Schmuttenmaer C A 2000 *Phys. Rev. B* **62** 15764
[29] Paingad V C, Kunc J, Rejhon M, Rychetský I, Mohelský I, Orlita M and Kužel P 2021 *Adv. Funct. Mater.* **31** 2105763
[30] Jnawali G, Rao Y, Yan H and Heinz T F 2013 *Nano Lett.* **13** 524
[31] Tielrooij K J, Song J C W, Jensen S A, Centeno A, Pesquera A, Zurutuza Elorza A, Bonn M, Levitov L S and Koppens F H L 2013 *Nat. Phys.* **9** 248
[32] Tomadin A, Hornett S M, Wang H I, Alexeev E M, Candini A, Coletti C, Turchinovich D, Kläui M, Bonn M, Koppens F H L, Hendry E, Polini M and Tielrooij K J 2018 *Sci. Adv.* **4** eaar5313
[33] Mao H K, Chen X J, Ding Y, Li B and Wang L 2018 *Rev. Mod. Phys.* **90** 015007
[34] Zhang L, Tang Y, Khan A R, Hasan M M, Wang P, Yan H, Yildirim T, Torres J F, Neupane G P, Zhang Y, Li Q and Lu Y 2020 *Adv. Sci.* **7** 2002697
[35] Barboza A P M, Guimaraes M H D, Massote D V P, Campos L C, Barbosa Neto N M, Cancado L G, Lacerda R G, Chacham H, Mazzoni M S C and Neves B R A 2011 *Adv. Mater.* **23** 3014

[36] Xu F, Wu M Y, Safron N S, Roy S S, Jacobberger R M, Bindl D J, Seo J H, Chang T H, Ma Z and Arnold M S 2014 *Nano Lett.* **14** 682

[37] Ke F, Chen Y, Yin K, Yan J, Zhang H, Liu Z, Tse J S, Wu J, Mao H and Chen B 2019 *Proc. Natl. Acad. Sci. USA* **116** 9186

[38] Tao Z, Du J, Qi Z, Ni K, Jiang S and Zhu Y 2020 *Appl. Phys. Lett.* **116** 133101

[39] Pietryga J M, Zhuravlev K K, Whitehead M, Klimov V I and Schaller R D 2008 *Phys. Rev. Lett.* **101** 217401

[40] Meng X, Pandey T, Jeong J, Fu S, Yang J, Chen K, Singh A, He F, Xu X, Zhou J, Hsieh W P, Singh A K, Lin J F and Wang Y 2019 *Phys. Rev. Lett.* **122** 155901

[41] Ni K, Du J, Yang J, Xu S, Cong X, Shu N, Zhang K, Wang A, Wang F, Ge L, Zhao J, Qu Y, Novoselov K S, Tan P, Su F and Zhu Y 2021 *Phys. Rev. Lett.* **126** 027402

[42] Zhang K, Xie J, Yang J, Jiang H, Zhang S, Zeng Z, Chen X, Wang T and Su F 2022 *Phys. Rev. B* **105** 195109

[43] Cantaluppi A, Buzzi M, Jotzu G, Nicoletti D, Mitrano M, Pontiroli D, Riccò M, Perucchi A, Di Pietro P and Cavalleri A 2018 *Nat. Phys.* **14** 837

[44] Fülöp J A, Pálfalvi L, Almási G and Hebling J 2010 *Opt. Express* **18** 12311

[45] Hirori H, Doi A, Blanchard F and Tanaka K 2011 *Appl. Phys. Lett.* **98** 091106

[46] Boubanga-Tombet S, Chan S, Watanabe T, Satou A, Ryzhii V and Otsuji T 2012 *Phys. Rev. B* **85** 035443

[47] Yamashita M and Otani C 2021 *Phys. Rev. Res.* **3** 013150

[48] Xu S, Huang D, Liu Z, Zhang K, Jiang H, Gou H, Zeng Z, Wang T and Su F 2021 *Opt. Express* **29** 14058

[49] Zhang K, Xie J, Yang J, Jiang H, Zhang S, Zeng Z, Chen X, Wang T and Su F 2022 *Phys. Rev. B* **105** 195109

[50] Gao B, Hartland G, Fang T, Kelly M, Jena D, Xing H Grace and Huang L 2011 *Nano Lett.* **11** 3184

[51] Betz A C, Vialla F, Brunel D, Voisin C, Picher M, Cavanna A, Madouri A, Fève G, Berroir J M, Plaçais B and Pallecchi E 2012 *Phys. Rev. Lett.* **109** 056805

[52] Song J C W, Reizer M Y and Levitov L S 2012 *Phys. Rev. Lett.* **109** 106602

[53] Winnerl S, Orlita M, Plochocka P, Kossacki P, Potemski M, Winzer T, Malic E, Knorr A, Sprinkle M, Berger C, de Heer W A, Schneider H and Helm M 2011 *Phys. Rev. Lett.* **107** 237401

[54] Cao H, Aivazian G, Fei Z, Ross J, Cobden D H and Xu X 2016 *Nat. Phys.* **12** 236

[55] Dawlaty J M, Shivaraman S and Chandrashekhar M 2008 *Appl. Phys. Lett.* **93** 131905

[56] Brida D, Tomadin A, Manzoni C, Kim Y J, Lombardo A, Milana S, Nair R R, Novoselov K S, Ferrari A C, Cerullo G and Polini M 2013 *Nat. Commun.* **4** 1987

[57] Moody G, Kavir Dass C, Hao K, Chen C H, Li L J, Singh A, Tran K, Clark G, Xu X, Berghäuser G, Malic E, Knorr A and Li X 2015 *Nat. Commun.* **6** 8315

[58] Wu Y, Yin X, Hasaien J, Ding Y and Zhao J 2020 *Chin. Phys. Lett.* **37** 047801